Hong Kong Baptist University
HKBU Institutional Repository

HKBU Staff Publication

2016

Isotropy test for spatial point processes using stochastic reconstruction

Ka Yiu Wong
Hong Kong Baptist University, wky313@gmail.com

Sung Nok Chiu
Hong Kong Baptist University, snchiu@hkbu.edu.hk

This document is the authors' final version of the published article.
Link to published article: http://dx.doi.org/10.1016/j.spasta.2015.12.002

APA Citation

Wong, K., & Chiu, S. (2016). Isotropy test for spatial point processes using stochastic reconstruction. *Spatial Statistics* (15), 56-69. https://doi.org/10.1016/j.spasta.2015.12.002

This Journal Article is brought to you for free and open access by HKBU Institutional Repository. It has been accepted for inclusion in HKBU Staff Publication by an authorized administrator of HKBU Institutional Repository. For more information, please contact repository@hkbu.edu.hk.

Isotropy Test for Spatial Point Processes using Stochastic Reconstruction

Ka Yiu Wong[a], Sung Nok Chiu[a]

[a]*Department of Mathematics, Hong Kong Baptist University, Kowloon Tong, Hong Kong*

Abstract

We develop a model-free isotropy test for spatial point patterns. The proposed test statistic assesses the discrepancy between the uniform distribution and the empirical normalised reduced second-order moment measure of a sector of increasing central angle. The null distribution of the test statistic is approximated by the empirical distribution obtained from bootstrap-type samples, which are generated by a stochastic procedure reconstructing independent isotropic patterns that resemble the spatial structure of the given point pattern, without specifying any underlying model. Simulation studies show that, when compared with the asymptotic χ^2-test by Guan et al. (2006), the powers of the proposed test are more robust to different choices of user-chosen parameter. When applied to patterns of amacrine cells and Spanish towns, the bootstrap-type test clearly suggests rejection for the former and

Email addresses: wky313@gmail.com (Ka Yiu Wong), snchiu@hkbu.edu.hk (Sung Nok Chiu)

not rejection for the latter, while the asymptotic χ^2-test is not conclusive in either case.

Keywords: Anisotropy, Bootstrap, Model-free, Orientation analysis, Reduced second-order moment measure

1. Introduction

An often made assumption in spatial point pattern analysis is that an observed pattern is a realisation of a motion-invariant spatial point process. A spatial process is motion-invariant if it is stationary and isotropic. The distribution of a stationary process is invariant under translations while that of an isotropic process is invariant under rotations. A stationary process is not necessarily isotropic and a non-stationary process can be isotropic with respect to rotations about a fixed location (e.g. Byth, 1981).

Typically, stationarity and isotropy are either justified by non-statistical arguments or checked by assessing the goodness of fit of certain classes of models. However, non-statistical justification is not always unarguable and goodness-of-fit tests are often not powerful in detecting lack of fit caused by non-stationarity or anisotropy. Moreover, any lack of fit of a stationary isotropic model cannot be regarded as evidence against stationarity or

isotropy. Thus, in many applications model-free tests for stationarity and isotropy would be valuable.

For stationarity, Guan (2008) and Chiu and Liu (2013) developed model-free asymptotic tests, based on the discrepancies between observed and expected numbers of points in expanding rectangular regions within a rectangular sampling window. When applying the tests to the longleaf pine data of Platt et al. (1988), which showed no strong evidence of lack of fit if the pattern is modelled by some stationary cluster processes (Stoyan and Stoyan, 1996; Ghorbani, 2013), Chiu and Liu (2013) obtained small p-values that led to a clear rejection of stationarity. Zhang and Zhou (2014) introduced another stationarity test that can be applied to non-rectangular sampling windows.

For isotropy, Guan et al. (2006) introduced a model-free statistic comparing the sample second-order product density at user-chosen lag vectors in some prescribed directions. Using the asymptotic normality of the density estimator, they showed that the limiting null distribution of their statistic is χ^2 with r degrees of freedom, where $r + 1$ is the number of *a priori* chosen directions for comparison. However, in real applications of their test, there are several practical issues. First, their simulation results reveal that the

power of the test is quite sensitive to the bandwidth for the kernel estimator of the second-order product density and to the magnitudes of the lag vectors, even if these values are chosen within their recommended ranges. Second, if one wants to compare more directions, the price to pay is a larger value for the degrees of freedom, which may lead to lower powers. Third, their statistic involves the inverse of an empirical covariance matrix, which may be ill-conditioned. Nevertheless, they offered some helpful suggestions from their experience on these issues.

Figure 1(a) shows the point pattern formed by the locations of 69 Spanish towns in a square sampling window; see Comas et al. (2011), Delicado et al. (2010), Illian et al. (2008), Ripley (1977, 1988), and Stoyan et al. (1995). The pattern in Figure 1(b) is a bivariate pattern of 152 and 142 points, respectively, of two different types of displaced amacrine cells in the retina of a rabbit; the "on" and "off" cells represent the types that transmit information when a light is "on" and "off", respectively; see Diggle (2013) and Illian et al. (2008). In the literature these two patterns are modelled and analysed as realisations of motion-invariant processes. For the stationarity hypothesis, applying the tests in Guan (2008) and Chiu and Liu (2013) to each pattern does not suggest rejection. For isotropy, however, visual inspection

of the empirical densities $\hat{\vartheta}(t)$ of the nearest-neighbour orientation distribution (Illian et al., 2008, Section 4.5.2) in Figure 2 clearly suggests a bimodal distribution for the patterns of the "on" and "off" amacrine cells. When we ignore the "on" or "off" marks and consider the pattern of all 294 unmarked cells, the empirical density, which is flattened a bit but whose standard error should also be reduced because of a larger sample size, still reveals a bimodal shape. For the pattern of Spanish towns, because there are only 69 points, it seems reasonable to say that the empirical density deviates not much from the uniform density.

However, when we applied the isotropy test by Guan et al. (2006) to these patterns with parameter values chosen within the recommended ranges, the results are inconclusive because the p-values, depending on the magnitude of the lag vectors and the bandwidth, range from 0.0000 to 1.0000 for the Spanish towns, from 0.0322 to 0.7216 for the unmarked amacrine cells, from 0.0029 to 0.9544 for the "on" amacrine cells, and from 0.0054 to 0.9197 for the "off" amacrine cells. Such a wide range of p-values of a given pattern shows that in practice, we need an alternative test that requires fewer user-chosen parameters and is less sensitive to the choice of the values for these parameters. As we can see in Section 5, our approach described below (which

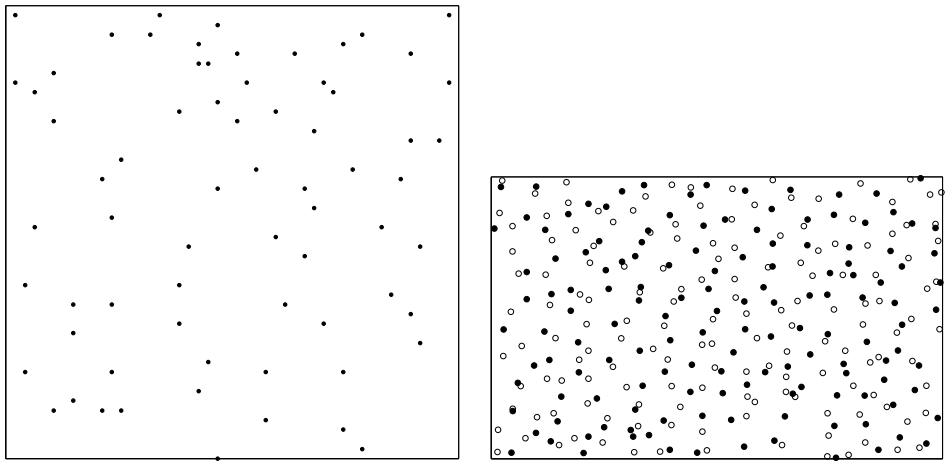

(a) (b)

Figure 1: Point patterns formed by (a) the locations of 69 Spanish Towns in a $40 \times 40\,\text{miles}^2$ window (source of data: `R` package `spatial`) and (b) the locations of 152 "on" amacrine cells (represented by bullets $\bullet$) and 142 "off" amacrine cells (represented by circles $\circ$) in a $1060 \times 662\,\mu\text{m}^2$ window (source of data: `R` package `spatstat`).

is not based on $\hat{\vartheta}(t)$), when applied to these two data sets, is able to offer robust and strong evidence to reject the isotropy hypothesis for the amacrine cells and to give consistently large p-values for the Spanish towns.

The idea of the test statistic proposed in this paper comes from the orientation analysis introduced in Ohser and Stoyan (1981), who considered the normalised reduced second-order moment measure, as a function of the central angle, of a sector with fixed radius and of a sector ring, which is the set difference of two sectors centred at the origin making the same angle with respect to the x-axis but with two different fixed radii; see also Illian

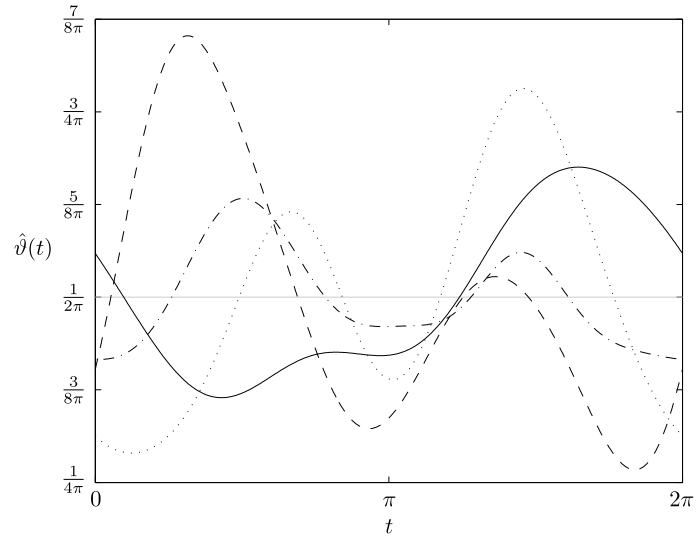

Figure 2: Kernel smoothed empirical density $\hat{\vartheta}(t)$ of the nearest-neighbour orientation distribution of the Spanish towns (solid line), the amacrine cells (dash-dot line), the "on" amacrine cells (dotted line), and the "off" amacrine cells (dashed line).

et al. (2008, Section 4.5.3), Stoyan et al. (1995, Section 4.5) and Stoyan and Stoyan (1994, Sections 14.10 and 15.4.5). Our new test statistic assessing the discrepancy between the uniform distribution and the empirical normalised reduced second-order moment measure of a sector of fixed radius with increasing central angle. Anisotropy would result in a large discrepancy. The null distribution of the discrepancy is, however, unknown and is not possible to be estimated by parametric bootstrap because the isotropy null hypothesis is not specific enough to allow simulation of realisations. We consider using stochastic reconstruction (Illian et al., 2008, Section 6.7) to estimate

the p-values. Such an approach has been shown to be able to yield more accurate estimates for point process summary characteristics (Tscheschel and Chiu, 2008). The simulation study in Section 4 shows that we can achieve empirical sizes that are close to the nominal level, while the powers are as high as, if not higher than, those of Guan et al. (2006) and more importantly, are much less sensitive to the choice of the sole user-chosen parameter in the test statistic, namely the radius of the sector.

The paper is organised as follows. Section 2 introduces the test statistic and Section 3 explains how to generate motion-invariant point patterns that closely resemble the spatial structure of the given data without specifying any underlying model. We compare our test with the test proposed in Guan et al. (2006) by extensive simulation in Section 4. The last section concludes the paper by applying the tests to the above two examples to demonstrate the advantages of our approach over Guan et al. (2006).

2. Asymptotic χ^2-test

Denote by Φ a point process in $\mathbb{R}^d$. For any Borel $A \subset \mathbb{R}^d$, $\Phi(A)$ is the random number of the points of the process in A. The intensity function

$\lambda(\boldsymbol{x})$ and second-order product density $\rho^{(2)}(\boldsymbol{x}, \boldsymbol{y})$ are functions satisfying

$$\mathbf{E}\{\Phi(A)\} = \int_A \lambda(\boldsymbol{x})\,\mathrm{d}\boldsymbol{x} \quad \text{and} \quad \mathbf{E}\{\Phi(A_1)\Phi(A_2)\} = \int_{A_1}\int_{A_2} \rho^{(2)}(\boldsymbol{x}, \boldsymbol{y})\,\mathrm{d}\boldsymbol{x}\mathrm{d}\boldsymbol{y}\,,$$

where A_1 and A_2 are disjoint. For the rest of this paper, the point process Φ is assumed to be stationary. Consequently, $\lambda(\boldsymbol{x}) = \lambda$ and, with slight abuse of notation, $\rho^{(2)}(\boldsymbol{x}, \boldsymbol{y}) = \rho^{(2)}(\boldsymbol{x} - \boldsymbol{y})$. If Φ is also isotropic, the second-order product density depends solely on $\|\boldsymbol{x} - \boldsymbol{y}\|$. Consider a vector $\boldsymbol{G}$ of the second-order product densities at some user-chosen lag vectors $\boldsymbol{t}_i$ of equal length. We estimate $\boldsymbol{G}$ by $\hat{\boldsymbol{G}}$, which is the vector of $\hat{\rho}^{(2)}(\cdot)$ at the same lags as $\boldsymbol{G}$, where

$$\hat{\rho}^{(2)}(\boldsymbol{t}_i) = \int_{\boldsymbol{x}\in W}\int_{\boldsymbol{y}\in W} \frac{w\{(\boldsymbol{t}_i - \boldsymbol{x} + \boldsymbol{y})/h\}}{h^2|W \cap (W - \boldsymbol{x} + \boldsymbol{y})|}\mathbf{1}(\boldsymbol{x} \neq \boldsymbol{y})\Phi(\mathrm{d}\boldsymbol{x})\Phi(\mathrm{d}\boldsymbol{y})\,,$$

in which W is the sampling window, $|X|$ the Lebesgue measure of $X \subset \mathbb{R}^d$, $w(\cdot)$ a symmetric kernel function of finite support, and h the bandwidth. Denote by $\boldsymbol{\Sigma}$ the covariance matrix of $\hat{\boldsymbol{G}}$ and by $\hat{\boldsymbol{\Sigma}}$ a consistent estimator of $\boldsymbol{\Sigma}$. For any point process satisfying certain moment conditions and a weak

dependence assumption stated in Guan et al. (2006), the test statistic

$$TS = h^2|W|(\boldsymbol{A}\hat{\boldsymbol{G}})^\top(\boldsymbol{A}\hat{\boldsymbol{\Sigma}}\boldsymbol{A}^\top)^{-1}(\boldsymbol{A}\hat{\boldsymbol{G}})$$

is asymptotically χ^2 distributed with rank($\boldsymbol{A}$) degrees of freedom as $W \uparrow \mathbb{R}^d$, under the null hypothesis that $\mathbf{E}(\boldsymbol{A}\hat{\boldsymbol{G}}) = \mathbf{0}$ and some regularity conditions on W and h. The matrix $\boldsymbol{A}$ is some fixed full row rank matrix chosen to compare $\hat{\rho}^{(2)}(\cdot)$ at different directions, and this null hypothesis is a consequence of the isotropy assumption.

The power of the test strongly depends on the choice of the bandwidth h and the user-chosen lag vectors $\boldsymbol{t}_i$. Simulation studies by Guan et al. (2006) led to the following guidelines. The recommended choice of $\|\boldsymbol{t}_i\|$ is some value about one third to a half of the dependence range of the point process. The value of the bandwidth h should be selected to meet two criteria: sufficiently many point pairs would be included in the calculation of each $\hat{\rho}^{(2)}(\boldsymbol{t}_i)$ and no overlapping point pairs would be used to calculate $\hat{\rho}^{(2)}(\cdot)$ in different directions.

They also introduced a data-driven method to estimate the optimal bandwidth by minimising the mean squared error of $\hat{\rho}^{(2)}(\boldsymbol{t}_i)$, but the computa-

tion would be very intensive and was not implemented in their simulation. As a remark, Guan (2007a,b) proposed further data-driven cross-validation approaches for bandwidth selection in the estimation of $\rho^{(2)}(\cdot)$. However, in our context, as we can see from the case studies in Section 5, at the same value for $\|\boldsymbol{t}_i\|$, a small difference in the bandwidth value (e.g. 0.0904 vs 0.0950 in the pattern of 142 "off" amacrine cells in the sampling window $[0, 1.6012085] \times [0, 1]$) can result in a substantial difference in the p-value (0.8293 vs 0.2128). Thus, using more bandwidth selection methods will only lead to more possible values for the users to choose but not result in more robust p-values. For a fair comparison, we follow the approach in Guan et al. (2006) and do not include any data-driven methods for bandwidth selection in our simulation.

The consistent estimator $\hat{\boldsymbol{\Sigma}}$ used is computed by a sub-sampling approach, instead of by a plug-in estimator. The observation window W is divided into k subblocks W_ℓ that are not necessarily non-overlapping and such that approximately $cn^{1/4}$ points are included in each subblock. Guan et al. (2006) suggested that $c \approx 0.8$ would often be a good choice. The shape and orientation of each subblock are the same as those of W. The (i, j)th element of

$\hat{\mathbf{\Sigma}}$ is given by

$$\frac{1}{kf}\sum_{\ell=1}^{k}\left\{\tilde{\rho}_{\ell}^{(2)}(\boldsymbol{t}_i)-\bar{\rho}^{(2)}(\boldsymbol{t}_i)\right\}\left\{\tilde{\rho}_{\ell}^{(2)}(\boldsymbol{t}_j)-\bar{\rho}^{(2)}(\boldsymbol{t}_j)\right\},$$

where $f = 1 - |W_\ell|/|W|$ is a finite sample bias correction factor, $\tilde{\rho}_{\ell}^{(2)}(\boldsymbol{t})$ the estimated second-order product density computed using only the points in the subblock W_ℓ, and $\bar{\rho}^{(2)}(\boldsymbol{t})$ the mean of all $\tilde{\rho}_{\ell}^{(2)}(\boldsymbol{t})$, $\ell = 1, \ldots, k$. No recommended value for k is proposed in Guan et al. (2006) and in our simulation study we follow their program code and use 20×20 regularly spaced subblocks for $\hat{\mathbf{\Sigma}}$.

The computation of $\hat{\rho}_{\ell}^{(2)}(\boldsymbol{t})$ involves another bandwidth to be used for the estimation in each subblock, and it may be difficult to select a value that would satisfy the two selection criteria mentioned above because a subblock often contains only a few points. Our simulation shows that in practice, the condition number of $\hat{\mathbf{\Sigma}}$ is very sensitive to the value of this bandwidth, and hence one may have an unstable inverse $\hat{\mathbf{\Sigma}}^{-1}$ for computing TS. In the simulation and the case studies below, following Guan et al. (2006), we employ the uniform kernel and use the same bandwidth for both $\hat{\rho}^{(2)}(\cdot)$ and

$\hat{\rho}_\ell^{(2)}(\cdot)$; the matrix

$$\boldsymbol{A} = \begin{bmatrix} 1 & -1 & 0 & 0 \\ 1 & 0 & -1 & 0 \\ 1 & 0 & 0 & -1 \end{bmatrix}$$

is used to compare the direction of the x-axis to the directions of $\pi/4$, $\pi/2$ and $3\pi/4$ with respect to the x-axis.

3. Bootstrap-type test

3.1. Test statistic

Consider the reduced second-order moment measure $\mathcal{K}$, which is defined by

$$\lambda\mathcal{K}(A) = \mathbf{E}_o\{\Phi(A\backslash\{o\})\}\,, \quad \text{for Borel } A \subseteq \mathbb{R}^d,$$

where $\mathbf{E}_o$ is the expectation with respect to the Palm distribution of Φ. In the planar case, consider $A = S(r, \theta, \psi)$ the sector of radius r centred at the origin whose two radii make angles $\theta + \psi$ and ψ with respect to the x-axis, where $0 \leq \theta \leq \pi$, and let $K_r(\theta, \psi) = \mathcal{K}(S(r, \theta, \psi))$. Generalisation to higher dimensional cases is, though straightforward, clumsy and so would not be explicitly spelt out here.

At fixed r and ψ, the ratio $F_{r,\psi}(\theta) = K_r(\theta,\psi)/K_r(\pi,0)$ is the distribution function of uniform on $[0,\pi]$ if Φ is isotropic; see Illian et al. (2008, Section 4.5). We now introduce a test statistic by comparing $F_{r,\psi}(\theta)$ with the empirical $\hat{F}_{r,\psi}(\theta)$ at fixed r under all θ and ψ.

Define

$$d_{r,\psi} = \sup_{\theta\in[0,\pi)} \left| \frac{\theta}{\pi} - \hat{F}_{r,\psi}(\theta) \right|$$

to measure, in L^∞-norm, the difference between the uniform distribution and the empirical function $\hat{F}_{r,\psi}(\cdot)$ at fixed r and ψ, and let

$$T_r = \sup_{\psi\in[0,\pi)} d_{r,\psi}.$$

For a fixed r, denote by $\{\theta_r^{(i)}\}_{i=1}^m$ a sequence of angles, sorted in ascending order and measured with respect to the x-axis, between pairs of points in the observed point pattern with pairwise distance smaller than or equal to r. Let $f_r^{(i)} = \hat{F}_{r,0}(\theta_r^{(i)})$, $i = 1,\ldots,m$, and define $f_r^{(0)} = f_r^{(m)}$. The empirical function $\hat{F}_{r,\psi}(\theta)$ is a step function with jumps at $\theta = \theta_r^{(i)} - \psi + \pi\mathbf{1}(\theta_r^{(i)} < \psi)$, $i = 1,\ldots,m$. The supremum of $d_{r,\psi}$ for all $\psi \in [\theta_r^{(j-1)}, \theta_r^{(j)}]$ occurs at either $\psi = \theta_r^{(j-1)}$ or $\psi = \theta_r^{(j)}$, $j = 2,\ldots,m-1$, and for all $\psi \in [0,\theta_r^{(1)}] \cup [\theta_r^{(m)},\pi]$, at

either $\psi = \theta_r^{(1)}$ or $\psi = \theta_r^{(m)}$. Thus, the test statistic T_r can be expressed as

$$T_r = \max_{1\le i\le m}\max_{1\le j\le m}\left\{\begin{array}{l}\left|\dfrac{\theta_r^{(i)}-\theta_r^{(j)}}{\pi}+\mathbf{1}(\theta_r^{(i)}<\theta_r^{(j)})-\dfrac{f_r^{(i)}-f_r^{(j-1)}}{f_r^{(m)}}-\mathbf{1}(f_r^{(i)}\le f_r^{(j-1)})\right|,\\ \left|\dfrac{\theta_r^{(i)}-\theta_r^{(j)}}{\pi}+\mathbf{1}(\theta_r^{(i)}\le\theta_r^{(j)})-\dfrac{f_r^{(i-1)}-f_r^{(j-1)}}{f_r^{(m)}}-\mathbf{1}(f_r^{(i-1)}\le f_r^{(j-1)})\right|,\\ \left|\dfrac{\theta_r^{(i)}-\theta_r^{(j)}}{\pi}+\mathbf{1}(\theta_r^{(i)}<\theta_r^{(j)})-\dfrac{f_r^{(i)}-f_r^{(j)}}{f_r^{(m)}}-\mathbf{1}(f_r^{(i)}<f_r^{(j)})\right|,\\ \left|\dfrac{\theta_r^{(i)}-\theta_r^{(j)}}{\pi}+\mathbf{1}(\theta_r^{(i)}\le\theta_r^{(j)})-\dfrac{f_r^{(i-1)}-f_r^{(j)}}{f_r^{(m)}}-\mathbf{1}(f_r^{(i-1)}<f_r^{(j)})\right|\end{array}\right\}.$$

Based on our simulation results, in applications we suggest choosing r as a half to two thirds of the dependence range of the point process.

3.2. Generating bootstrap samples by reconstruction

Motion-invariant point patterns that resemble the spatial structure of a given sample of n points observed in W could be generated using stochastic reconstruction, which is developed by Tscheschel and Stoyan (2006). Without specifying any theoretical model with finitely many parameters for the observed pattern, the reconstruction procedure generates point patterns with empirical summary characteristics close to the prescribed summary characteristics of the observed pattern.

The algorithm starts with an arbitrary finite point pattern Φ_0 of exactly

n points in W. A sequence of point patterns $\Phi_1, \Phi_2, \ldots$ is generated in W as follows. A point in Φ_i is randomly chosen and replaced by a new point that is independent and uniformly distributed in W. Denote the new pattern by Φ_i', which will be accepted as Φ_{i+1} if there is a decrease in the energy function that measures the discrepancy in the prescribed summary characteristics between two point patterns. For the choice of summary characteristics, Illian et al. (2008, Section 6.7) favours the spherical contact distribution function $H_s(\cdot)$ and the L-function, which is a normalised version of Ripley's K-function, and Tscheschel and Stoyan (2006) praises the kth nearest-neighbour distance distribution functions $D_k(\cdot)$. Either choice has been shown to be good. However, our test statistic is closely related to Ripley's K-function, because both are constructed from the reduced second-order moment measure, it is more reasonable not to use the L-function in the energy function. Hence, $D_k(\cdot)$ are used.

More precisely, define the energy function of Φ_i as

$$U(\Phi_i) = \sum_{k=1}^{I} \int_0^{r_0} \left\{ \hat{D}_k(r; \Phi) - \hat{D}_k(r; \Phi_i) \right\}^2 \mathrm{d}r + \int_0^{r_0} \left\{ \hat{N}^+(r; \Phi) - \hat{N}^+(r; \Phi_i) \right\}^2 \mathrm{d}r$$

for some positive I and r_0, where $\hat{D}_k(r; \Psi)$ is an estimate of $D_k(r)$ for Ψ and $\hat{N}^+(r; \Psi)$ is an estimate of the specific planar convexity number of the random

set formed by the union of closed balls of radius r centred at the points of Ψ, where Ψ is a point pattern. The specific planar convexity number is one of the morphological functions introduced by Mecke (2000) and is very informative for the statistical description of random sets; the inclusion of it in the energy function improves the powers of the test in our simulation study. Because Φ and Φ_i are observed only in the sampling window W, correction for edge-effects is necessary. If W is rectangular, periodic boundary conditions may simply be used for the estimation. If W is non-rectangular, other edge-effects correction methods may be used; see Chiu et al. (2013, Section 4.7.6). An estimate of $\hat{N}^+$ can be the count of lower tangent points (Chiu et al., 2013, p. 294).

The pattern Φ_{i+1} is defined as

$$\Phi_{i+1} = \begin{cases} \Phi_i', & \text{if } U(\Phi_i') < U(\Phi_i), \\ \\ \Phi_i, & \text{otherwise.} \end{cases}$$

The iteration process stops when either the number of iterations i has reached the maximum number of iterations M or $U(\Phi_{i-s}) - U(\Phi_i) < \varepsilon$ for some small ε and large s. The resultant pattern is called a reconstructed pattern from

the observed Φ.

Our experience suggests that I is about 5% of the total number n of points in W but should not be smaller than 5, the upper limit r_0 of the integral is chosen as the reciprocal of the intensity but should not be smaller than 5% and not greater than 25% of the shortest side of W. The parameters for termination are $M = 10^6$, $\varepsilon = 10^{-8}$, and $s = 1000$.

Although the test statistic T_r has only one user-chosen parameter, the reconstruction procedure, which is used to get an approximate of the p-value, requires further user-chosen parameters. However, the purpose of the reconstruction is only to produce stochastic patterns that resemble the spatial structure of the given pattern, and mild changes in these reconstruction parameters will not lead to substantial changes in the spatial structure of the reconstructed patterns. The bootstrap p-value explained in the next section, based on observations of our extensive simulation studies, is practically robust to mild deviations of these parameters from the above suggested values. Thus, it is fair to restrict our discussion of T_r to only the choice of r but not the reconstruction parameters.

3.3. Bootstrap p-value

Each reconstructed pattern from the observed Φ can be regarded as a (pseudo) bootstrap sample under the isotropy hypothesis, and consequently the bootstrap p-value can be obtained as usual: for a given observed pattern, in total R reconstructed patterns are generated independently, and for a fixed r and $i = 1, \ldots, R$, denote by $T_r^{(i)}$ the test statistic value obtained in the ith pattern; the bootstrap p-value is defined by

$$p_{\text{bootstrap}} = \frac{\#\{i : T_r^{(i)} \geq T_r\} + 1}{R + 1},$$

where T_r is the test statistic value obtained in the given pattern. Using $R = 99$ is generally adequate for practical purpose (Davison and Hinkley, 1997, p. 156).

It should be remarked that the use of stochastic reconstruction to generate bootstrap samples is not limited to the isotropy test; in principle it can be applied to any model-free tests in spatial point pattern analysis. However, the energy function $U(\cdot)$ used in the previous section does not consider any directional properties, because isotropic samples are needed. If the given pattern is not necessarily isotropic under the null hypothesis, such as the stationar-

ity test mentioned in Section 1, then a more sophisticated energy function incorporating some directional summary characteristics must be used.

4. Simulation

For each model described below, 500 realisations were generated in the sampling window $W = [0, 20]^2$ as observed patterns. The parameters of the asymptotic χ^2-test were determined according to the recommendation in Guan et al. (2006). For the bootstrap-type test, the p-values were calculated based on $R = 99$ independent reconstructed patterns. All integrals in the energy function were approximated by the corresponding right Riemann sums, where the interval $[0, r_0]$ was partitioned into J equal parts, and J need not be very large because the integrands may remain unchanged for a small increment in r. For the results reported in this section, the value of J and the parameters used in the energy function for the reconstruction were (i) for patterns with on the average 400 points, $J = 50$, $I = 20$ and $r_0 = 1$, and (ii) for patterns with on the average 30 points, $J = 20$, $I = 5$ and $r_0 = 5$.

4.1. Models

Poisson cluster processes and Gibbs hard-core processes were simulated to investigate the empirical rejection rates of the tests.

For cluster processes, we followed Guan et al. (2006). A stationary Poisson process with intensity $\rho/400$ was first generated as parent locations. The numbers of offsprings of each parent were independent Poisson random variables with mean μ. The vector to an offspring from its parent was independently distributed with density

$$f(\boldsymbol{t}) = \frac{1}{2\pi\sigma^2 \det(\boldsymbol{B})^{-1}} \exp(-\|\boldsymbol{B}\boldsymbol{t}\|^2/2\sigma^2)\,,$$

where

$$\boldsymbol{B} = \begin{bmatrix} 1 & 0 \\ 0 & p \end{bmatrix} \begin{bmatrix} \cos\theta & \sin\theta \\ -\sin\theta & \cos\theta \end{bmatrix}, \quad \text{for some } p \geq 1.$$

We chose $(\rho, \mu) = (100, 4)$, $(50, 8)$, $(15, 2)$ and $(5, 6)$. The spread of each cluster was controlled by the parameter $\sigma = 0.4$ and 0.6. The strength of anisotropy p was set as 1 (isotropy), $\sqrt{2}$, and 2, while the major direction of anisotropy θ was fixed at $\pi/3$ with respect to the x-axis. A simulated realisation of this anisotropic cluster process is shown in Figure 3(a). The same as in Guan et al. (2006), we took 4σ as the dependence range for the determination of the magnitude of the lag vectors $\boldsymbol{t_i}$ and the radius r of the sector in the test statistics TS and T_r, respectively.

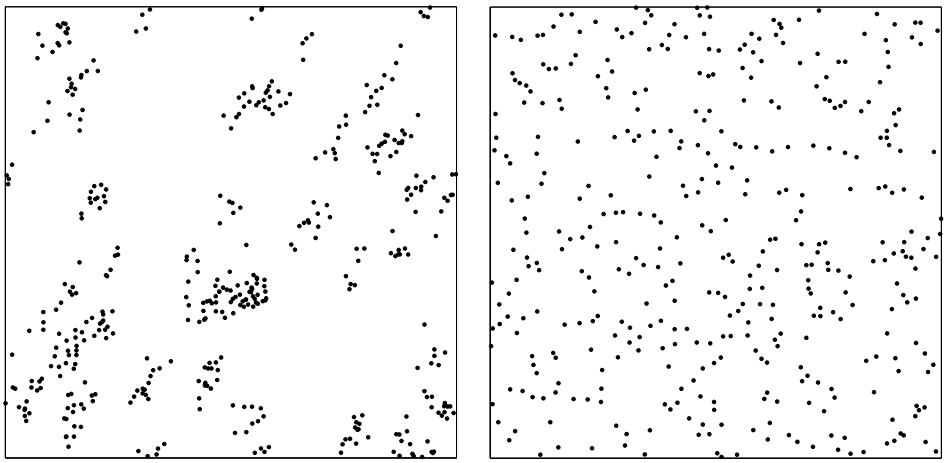

(a) (b)

Figure 3: Simulated patterns of (a) the anisotropic Poisson cluster process with $(\rho, \mu) = (50, 8)$, $\sigma = 0.6$ and $p = 2$, and (b) the anisotropic Gibbs hard-core process with $\xi = 400$, $\delta = 0.3$ and $p = 2$.

In addition to cluster processes, we considered Gibbs hard-core process with exactly ξ points, whose locations were simulated according to the density

$$f_\xi(\boldsymbol{x}_1, \ldots, \boldsymbol{x}_\xi) = \exp\left(-\sum_{i=1}^{\xi-1}\sum_{j=i+1}^{\xi} \phi(\|\boldsymbol{B}(\boldsymbol{x}_i - \boldsymbol{x}_j)\|)\right) \Big/ Z_\xi \,,$$

with normalising factor Z_ξ and the same matrix $\boldsymbol{B}$ as above, and

$$\phi(\|\boldsymbol{B}(\boldsymbol{x} - \boldsymbol{y})\|) = \begin{cases} \infty \,, & \text{if } \|\boldsymbol{B}(\boldsymbol{x} - \boldsymbol{y})\| \le \delta, \\ 0 \,, & \text{otherwise.} \end{cases}$$

In the simulation, we took $\xi = 400$ and 30. Though the Gibbs hard-core pro-

cess with a fixed number of points is not stationary, under periodic boundary conditions the simulated samples look like stationary (Chiu et al., 2013, p. 186), and in our simulation all samples passed the stationarity tests by Guan (2008) and Chiu and Liu (2013). The values of p and θ were the same as those of the Poisson cluster process above. The fixed hard-core distance was chosen to be $\delta = 0.2$, 0.3 for $\xi = 400$, and $\delta = 2$, 3 for $\xi = 30$. Visual inspection of $\hat{\rho}^{(2)}(r)$ suggested that the dependence range would be about 2δ to 3δ. A simulated realisation of this anisotropic hard-core process is shown in Figure 3(b), but the anisotropy is not visually evident.

4.2. Empirical results

Tables 1 and 2 show the empirical rejection rates of the bootstrap-type test and the asymptotic χ^2-test applied to Poisson cluster patterns and Gibbs hard-core patterns at the 5% nominal level.

For the asymptotic χ^2-test statistic, Guan et al. (2006) recommended that the values of $\|\boldsymbol{t}\|$ should be about one third to a half of the dependence range and the bandwidth h should be chosen to include more than 200 point pairs for the calculation of each $\hat{\rho}^{(2)}(r)$; in this simulation study, $\|\boldsymbol{t}\|$ ranged from a quarter to two thirds of the dependence range, and for patterns with on the average 400 points, choosing $h \geq 0.2$ for the clustered patterns and

Table 1: Empirical rejection probabilities of the bootstrap-type test and the asymptotic χ^2-test applied to Poisson cluster patterns at the 5% nominal level

			Bootstrap-type test										Asymptotic χ^2-test											
													$h = 0.2$				$h = 0.4$				$h = 0.6$			
			r										$\|\boldsymbol{t}\|$											
p	σ	(ρ, μ)	2σ	2.1σ	2.2σ	2.3σ	2.4σ	2.5σ	2.6σ	2.7σ	2.8σ	2.9σ	1σ	1.5σ	2σ	2.5σ	1σ	1.5σ	2σ	2.5σ	1σ	1.5σ	2σ	2.5σ
1	0.6	$(50, 8)$	0.058	0.054	0.050	0.052	0.050	0.050	0.046	0.044	0.044	0.050	0.052	0.054	0.044	0.040	0.078	0.060	0.048	0.050	0.052	0.072	0.086	0.072
		$(5, 6)$	0.024	0.020	0.018	0.022	0.012	0.012	0.020	0.018	0.014	0.012												
$\sqrt{2}$	0.4	$(100, 4)$	0.298	0.324	0.344	0.360	0.362	0.378	0.370	0.372	0.384	0.376	0.138	0.260	0.290	0.216	0.306	0.378	0.406	0.258	0.364	0.388	0.352	0.286
		$(50, 8)$	0.522	0.550	0.576	0.602	0.604	0.598	0.612	0.622	0.604	0.596	0.242	0.458	0.542	0.356	0.540	0.624	0.620	0.440	0.538	0.584	0.538	0.434
		$(15, 2)$	0.038	0.038	0.040	0.042	0.040	0.042	0.046	0.038	0.038	0.044												
		$(5, 6)$	0.042	0.042	0.054	0.050	0.054	0.058	0.054	0.050	0.052	0.048												
	0.6	$(100, 4)$	0.186	0.204	0.210	0.234	0.228	0.222	0.226	0.220	0.220	0.204	0.108	0.130	0.108	0.106	0.134	0.214	0.190	0.130	0.204	0.246	0.226	0.144
		$(50, 8)$	0.324	0.328	0.348	0.352	0.342	0.340	0.344	0.342	0.332	0.324	0.120	0.212	0.222	0.148	0.200	0.330	0.346	0.218	0.304	0.388	0.338	0.226
		$(15, 2)$	0.034	0.038	0.034	0.036	0.038	0.042	0.046	0.046	0.042	0.052												
		$(5, 6)$	0.050	0.048	0.054	0.052	0.056	0.070	0.068	0.068	0.066	0.070												
2	0.4	$(100, 4)$	0.970	0.976	0.982	0.982	0.982	0.982	0.972	0.968	0.960	0.946	0.768	0.922	0.770	0.350	0.954	0.982	0.934	0.580	0.804	0.936	0.882	0.678
		$(50, 8)$	0.992	0.994	0.994	0.994	0.996	0.994	0.994	0.992	0.992	0.988	0.958	0.982	0.946	0.604	0.992	0.988	0.976	0.756	0.934	0.974	0.954	0.826
		$(15, 2)$	0.112	0.126	0.144	0.150	0.166	0.182	0.188	0.188	0.192	0.210												
		$(5, 6)$	0.220	0.248	0.258	0.262	0.310	0.294	0.310	0.316	0.314	0.302												
	0.6	$(100, 4)$	0.804	0.808	0.818	0.792	0.788	0.760	0.734	0.688	0.658	0.632	0.402	0.498	0.312	0.142	0.656	0.772	0.534	0.196	0.796	0.808	0.582	0.272
		$(50, 8)$	0.966	0.962	0.950	0.954	0.942	0.928	0.916	0.906	0.890	0.856	0.688	0.822	0.602	0.236	0.916	0.944	0.778	0.356	0.952	0.944	0.838	0.424
		$(15, 2)$	0.098	0.108	0.124	0.120	0.128	0.132	0.148	0.142	0.144	0.140												
		$(5, 6)$	0.202	0.212	0.212	0.236	0.246	0.256	0.260	0.262	0.268	0.252												

Table 2: Empirical rejection probabilities of the bootstrap-type test and the asymptotic χ^2-test applied to Gibbs hard-core patterns at the 5% nominal level

			Bootstrap-type test										Asymptotic χ^2-test											
													$h = 0.3$				$h = 0.5$				$h = 0.7$			
			r										$\|\boldsymbol{t}\|$											
p	ξ	δ	1.1δ	1.2δ	1.3δ	1.4δ	1.5δ	1.6δ	1.7δ	1.8δ	1.9δ	2δ	0.5δ	1δ	1.5δ	2δ	0.5δ	1δ	1.5δ	2δ	0.5δ	1δ	1.5δ	2δ
1	400	0.2	0.129	0.042	0.052	0.032	0.036	0.050	0.052	0.036	0.036	0.032	0.044	0.066	0.064	0.064	0.050	0.068	0.060	0.066	0.060	0.064	0.068	0.056
	30	2	0.040	0.038	0.038	0.040	0.046	0.062	0.060	0.066	0.064	0.056												
$\sqrt{2}$	400	0.2	0.112	0.102	0.088	0.084	0.066	0.054	0.042	0.050	0.036	0.040	0.064	0.048	0.072	0.058	0.048	0.070	0.062	0.064	0.078	0.074	0.070	0.076
		0.3	0.298	0.184	0.166	0.138	0.096	0.082	0.088	0.072	0.086	0.070	0.070	0.078	0.088	0.050	0.048	0.080	0.064	0.058	0.046	0.042	0.082	0.048
	30	2	0.056	0.044	0.056	0.060	0.042	0.060	0.056	0.044	0.058	0.060												
		3	0.134	0.096	0.098	0.088	0.092	0.102	0.074	0.082	0.092	0.096												
2	400	0.2	0.188	0.132	0.110	0.106	0.098	0.090	0.076	0.070	0.074	0.058	0.084	0.064	0.054	0.086	0.068	0.080	0.076	0.114	0.064	0.086	0.082	0.078
		0.3	0.324	0.244	0.190	0.154	0.114	0.100	0.098	0.088	0.078	0.078	0.112	0.094	0.080	0.070	0.058	0.088	0.052	0.102	0.092	0.078	0.080	0.074
	30	2	0.080	0.078	0.062	0.040	0.052	0.056	0.044	0.040	0.040	0.038												
		3	0.114	0.110	0.112	0.094	0.098	0.076	0.088	0.078	0.070	0.068												

$h \geq 0.3$ for the hard-core patterns could meet the 200 point pairs requirement. A wider range for $\|\boldsymbol{t}\|$ is presented here because Guan et al. (2006) simulated only Poisson cluster processes but we simulated also Gibbs hard-core processes, and so considering a wider range may be fairer to the χ^2-test when we compare the powers of the two tests for hard-core processes. For a pattern containing only 30 points or so, the number of point pairs used to calculate $\tilde{\rho}_\ell^{(2)}(\boldsymbol{t})$ in each subblock was not large enough to guarantee the existence of $\hat{\boldsymbol{\Sigma}}^{-1}$, and consequently, the test statistic TS of Guan et al. (2006) sometimes could not be calculated. Thus, for small samples, not only the asymptotic χ^2-approximation but also any finite-sample approximation (e.g. by stochastic reconstruction) of the p-values of TS are not always possible; no rejection rate based on the test statistic TS for patterns of small number of points was reported here.

For the bootstrap-type test, the results would be good for some r about a half to two thirds of the dependence range; values of r less than a half of the dependence range should not be recommended by our experience. For example, as we can see from Table 2, taking $r = 1.1\delta$ in the Gibbs hard-core process would result in a high type I error rate; however, the rate would drop quickly to the nominal level for $r \geq 1.2\delta$.

For isotropic (i.e. $p = 1$) patterns with large number of points, a comparison of the empirical type I error rates of the two tests in the cases considered suggests that both tests could reasonably control the empirical size of the tests at the 5% nominal level, but the asymptotic χ^2-test could sometimes be liberal, while the bootstrap-type test sometimes conservative. For clustered patterns with small number of points, the bootstrap-type test could be quite conservative (and the asymptotic χ^2 test may be inapplicable).

For the anisotropic clustered patterns considered, as expected, when p increases, σ decreases or μ increases, the anisotropy of the clusters would be easier to be detected. For the anisotropic hard-core patterns considered, the powers of the bootstrap-type test increase as p or δ increases, but the powers are not much higher than the type I error rates (this explains why the anisotropy in Figure 3(b) is not visually evident). Nevertheless, a general impression is that the bootstrap-type test would have lower type I error rates but higher powers than the asymptotic χ^2-test.

Both Table 1 in Guan et al. (2006) and our Tables 1 and 2 reveal a practical problem of the asymptotic χ^2-test, namely, the power of the test depends strongly on the choice of the magnitude $\|\boldsymbol{t}\|$ and the bandwidth h. In most of our simulated clustered patterns, the highest powers would be

achieved at $\|\boldsymbol{t}\| = 1.5\sigma$ or 2σ. This observation agrees with the choice of $\|\boldsymbol{t}\|$ recommended by Guan et al. (2006). In all simulated clustered patterns, $h = 0.2$ would yield the lowest powers as the numbers of point pairs used to calculate $\tilde{\rho}_{\ell}^{(2)}(\boldsymbol{t})$ are, though larger than 200, still small. For the cases with $\sigma = 0.4$ and $\sigma = 0.6$, the highest powers occur at $h = 0.4$ and $h = 0.6$ respectively. These empirical results are consistent with those reported in Guan et al. (2006). For the simulated hard-core patterns, none of the four chosen values for $\|\boldsymbol{t}\|$ is clearly better or worse than the others, and increasing to 2.5δ (not tabulated here) would only result in lower powers than those shown in Table 2.

On the other hand, the variation of powers of the bootstrap-type test under different choices of r seems small. In almost all simulated clustered patterns, the test using $r = 2\sigma$ or $r = 2.9\sigma$ would be the least powerful, and most of the time, the test would be the most powerful for r between 2.3σ and 2.7σ (i.e. 57.5% to 67.5% of the dependence range 4σ). For the simulated clustered patterns with 30 points, because of the conservativeness, the test was not successful in detecting the anisotropy when $p = \sqrt{2}$ but was able to do so when $p = 2$. For most simulated hard-core patterns, the lowest powers occur at $1.9\delta \leq r \leq 2\delta$, while the highest powers could be achieved when

$1.2\delta \leq r \leq 1.4\delta$ (the case $r = 1.1\delta$ should not be counted here because the high powers were "achieved" at the price of high type I error rates).

The highest powers of the asymptotic χ^2-test and the bootstrap-type test are close in all simulated clustered patterns with large numbers of points. However, the χ^2-test could have much lower powers if we choose bad values for its two parameters $\|\boldsymbol{t}\|$ and h. In contrast, our simulation shows that the bootstrap-type test would not be very sensitive to its sole parameter r. Moreover, compare the two tests in terms of their empirical sizes and powers in Table 2, we could conclude that the bootstrap-type test would be more capable of detecting anisotropy in Gibbs hare-core patterns than the asymptotic χ^2-test, which seems liberal but less powerful.

5. Applications to real data

The asymptotic χ^2-test and the bootstrap-type test were applied to the Spanish towns and amacrine cells shown in Figure 1, and the sampling window for the amacrine data has been re-scaled to $[0, 1.6012085] \times [0, 1]$ (so that 1 unit = 662 microns). For the amacrine cells, we consider the pattern of the cells marked as "on" and that of the cells marked as "off" separately and also consider the pattern of unmarked cells.

We followed Guan et al. (2006) and estimated the covariance matrix by the sub-sampling approach with the uniform kernel and the dependence range of a point pattern as the distance where the empirical isotropic second-order product density starts flattening out. The estimated dependence ranges of the Spanish towns and the patterns of amacrine cells are about 5 and 0.15, respectively. No recommended number of subblocks has been mentioned in Guan et al. (2006) and the p-values reported below are for the case that each sampling window containing n points is partitioned into non-overlapping subblocks such that each subblock contains approximately $cn^{1/4}$ points, where $c = 0.8$; this partition results in 5×5 regularly spaced subblocks for the Spanish towns, 9×9 for the unmarked amacrine cells, and 7×7 for the "on" or "off" amacrine cells. We also considered 20×20 regularly spaced subblocks as in the simulation study, as well as other choices of the number of subblocks; this will be discussed below.

Table 3 shows the p-values of the tests applied to these two data sets. For the asymptotic χ^2-test, the values of $\|\boldsymbol{t}\|$ and h were selected based on the recommendation in Guan et al. (2006). Four values of the bandwidth h were used; the first three values were chosen roughly to include about 200, 400 and 600 point pairs in the calculation of the empirical second-order product den-

sity, while the last one was determined by minimising the mean squared error as suggested in Guan et al. (2006). For the Spanish towns pattern, four more bandwidth values (such that 100, 150, 430 and 460 point pairs are included in the calculation; the first two values are outside the recommended range) are considered to show that the p-values are not monotonic but are unpredictable as the bandwidth increases. Four equally-spaced values from one third to a half of the dependence range were used for $\|\boldsymbol{t}\|$. For the bootstrap-type test the p-values were obtained by $R = 999$ reconstructed patterns, where the parameters in the reconstruction procedure were determined according to the recommendation given in the previous section and the interval $[0, r_0]$ was partitioned into $J = 30$ equal parts for the approximation of the integrals in the energy function.

For each of the four patterns of the Spanish towns, unmarked, "on" and "off' amacrine cells, respectively, we can see that the four (or eight) chosen values for the bandwidth h in the asymptotic χ^2-test led to four (or eight) rows of very different p-values; no row is in reasonable agreement with any other one. The same comment can be given to the four columns corresponding to the four chosen magnitudes $\|\boldsymbol{t}\|$ of the lag vectors. The lowest p-values for the four patterns are 0.0000, 0.0322, 0.0029 and 0.0054, but the highest

values are 1.00, 0.72, 0.95 and 0.92, respectively. There is no sensible way to draw any conclusions from the asymptotic χ^2-test. Moreover, for the Spanish towns data, the estimator $\hat{\mathbf{\Sigma}}$ is not invertible at $h = 9.5$ and $\|\boldsymbol{t}\| = 1.6667$, and hence no corresponding p-value is reported.

In contrast, the bootstrap-type test produces a row of rather robust small p-values for the three patterns of amacrine cells, giving a convincing justification for the rejection of the isotropy hypothesis. When applied to the Spanish towns, the test gives consistently large p-values, which show no evidence for rejecting the isotropy hypothesis.

We also used overlapping subblocks (of the same size as non-overlapping subblocks) whose lower-left corners form 10×10, 20×20 and 40×40 regular grids to estimate the covariance matrix. We do not report all the corresponding p-values here; as an illustration, Table 4 shows the p-values for the "on" amacrine cells at $h = 0.125$. The general observation is that the p-values corresponding to each of these three choices of the grid of the subblocks are different from those reported in Table 3, but relatively large/small p-values often remain relatively large/small. A notable exception to this general observation happens in the row corresponding to $h = 9.5$ for the Spanish towns, where 0.0000 and 1.0000 in Table 3 could change to 1.0000 and 0.0000, re-

spectively; such dramatic changes may be caused by the instability of the inverse of the covariance matrix estimator, which is close to singular for this small sample. In general, no matter how we choose the subblocks, the range of p-values for each pattern remains so wide that no conclusion can be drawn.

Proposing biological theory to explain the anisotropy in the amacrine cells is beyond the scope of this paper, but the rejection of isotropy suggests that modelling the marked and unmarked patterns by isotropic processes may be inadequate, even if the fitted models could pass some goodness-of-fit tests. Modelling them by anisotropic processes, such as geometric anisotropic Cox processes (Møller and Toftaker, 2014), may be more desirable.

Table 3: p-values of the bootstrap-type test and the asymptotic χ^2-test applied to the pattern of the 69 Spanish towns and the patterns of the 294 amacrine cells

Spanish towns															
	Bootstrap-type test										Asymptotic χ^2-test				
r	2.875	2.931	2.986	3.042	3.097	3.153	3.208	3.264	3.319	3.375	$h\backslash\|\boldsymbol{t}\|$	1.6667	1.9444	2.2222	2.5000
	0.811	0.785	0.764	0.734	0.635	0.609	0.595	0.573	0.531	0.459	4.0000	0.4587	0.7248	0.8967	0.1916
											4.5000	0.0041	0.0002	0.1845	0.6054
											6.0000	0.0160	0.3264	0.3099	0.1623
											7.5000	0.0017	0.0362	0.0168	0.0083
											7.7500	0.2873	0.5518	0.3067	0.0196
											8.0000	0.0000	0.0029	0.0128	0.0828
											9.5000	—	0.0000	0.0000	1.0000
											7.9065	0.0000	0.1010	0.0002	0.0030

Unmarked amacrine cells															
	Bootstrap-type test										Asymptotic χ^2-test				
r	0.086	0.088	0.090	0.091	0.093	0.095	0.096	0.098	0.100	0.101	$h\backslash\|\boldsymbol{t}\|$	0.0500	0.0583	0.0667	0.0750
	0.042	0.002	0.001	0.001	0.001	0.001	0.001	0.003	0.003	0.001	0.0450	0.1384	0.2777	0.0719	0.0322
											0.0600	0.2078	0.2489	0.4733	0.6264
											0.0750	0.4034	0.5060	0.5433	0.3404
											0.0386	0.7216	0.1746	0.1159	0.1088

"On" amacrine cells															
	Bootstrap-type test										Asymptotic χ^2-test				
r	0.086	0.088	0.090	0.091	0.093	0.095	0.096	0.098	0.100	0.101	$h\backslash\|\boldsymbol{t}\|$	0.0500	0.0583	0.0667	0.0750
	0.104	0.064	0.009	0.005	0.010	0.002	0.002	0.013	0.005	0.002	0.0950	0.6756	0.7490	0.6105	0.9544
											0.1250	0.2537	0.0553	0.0272	0.0029
											0.1500	0.0824	0.1061	0.2595	0.8549
											0.1568	0.2545	0.5549	0.2189	0.2871

"Off" amacrine cells															
	Bootstrap-type test										Asymptotic χ^2-test				
r	0.086	0.088	0.090	0.091	0.093	0.095	0.096	0.098	0.100	0.101	$h\backslash\|\boldsymbol{t}\|$	0.0500	0.0583	0.0667	0.0750
	0.004	0.006	0.004	0.005	0.002	0.001	0.001	0.001	0.001	0.003	0.0950	0.2128	0.2905	0.4658	0.9171
											0.1250	0.0054	0.0368	0.0192	0.1583
											0.1500	0.4108	0.4069	0.1722	0.4038
											0.0904	0.8293	0.5711	0.1895	0.5817

Table 4: p-values of the asymptotic χ^2-test at $h = 0.125$ applied to the pattern of the 152 "on" amacrine cells with different numbers of subblocks

No. of subblocks\$||\boldsymbol{t}||$	0.0500	0.0583	0.0667	0.0750
7×7 (non-overlapping)	0.2537	0.0553	0.0272	0.0020
10×10	0.0909	0.0780	0.0031	0.0025
20×20	0.1648	0.1618	0.0152	0.0128
40×40	0.1807	0.1725	0.0229	0.0165

Acknowledgements

We thank Yongtao Guan for providing us the Matlab code used for the simulation study in Guan et al. (2006) and the two referees for their valuable suggestions. This research was supported by GRF grants from the Research Grants Council of the Hong Kong Special Administrative Region, China (Project Nos. 200710 and 12301215).

References

Byth, K., 1981. θ-stationary point processes and their second-order analysis. Journal of Applied Probability 18, 864–878.

Chiu, S. N., Liu, K. I., 2013. Stationarity tests for spatial point processes using discrepancies. Biometrics 69, 497–507.

Chiu, S. N., Stoyan, D., Kendall, W. S., Mecke, J., 2013. Stochastic Geometry and its Applications, 3rd Edition. Wiley, Chichester.

Comas, C., Delicado, P., Mateu, J., 2011. A second order approach to analyse spatial point patterns with functional marks. Test 20, 503–523.

Davison, A. C., Hinkley, D. V., 1997. Bootstrap Methods and their Application. Cambridge University Press, New York.

Delicado, P., Giraldo, R., Comas, C., Mateu, J., 2010. Statistics for spatial functional data: some recent contributions. Environmetrics 21, 224–239.

Diggle, P. J., 2013. Statistical Analysis of Spatial and Spatio-Temporal Point Patterns, 3rd Edition. CRC Press, Boca Raton.

Ghorbani, M., 2013. Cauchy cluster process. Metrika 76, 697–706.

Guan, Y., 2007a. A composite likelihood cross-validation approach in selecting bandwidth for the estimation of the pair correlation function. Scandinavian Journal of Statistics 34, 336–346.

Guan, Y., 2007b. A least-squares cross-validation bandwidth selection approach in pair correlation estimations. Statistics & Probability Letters 77, 1722–1729.

Guan, Y., 2008. A KPSS test for stationarity for spatial point processes. Biometrics 64, 800–806.

Guan, Y., Sherman, M., Calvin, J. A., 2006. Assessing isotropy for spatial point processes. Biometrics 62, 119–125.

Illian, J., Penttinen, A., Stoyan, H., Stoyan, D., 2008. Statistical Analysis and Modelling of Spatial Point Patterns. Wiley, Chichester.

Mecke, K., 2000. Additivity, convexity, and beyond: applications of Minkowski Functionals in statistical physics. In: Mecke, K. R., Stoyan, D. (Eds.), Statistical Physics and Spatial Statistics: the Art of Analyzing and Modeling Spatial Structures and Pattern Formation. Lecture Notes in Physics 554. Springer-Verlag, Berlin, pp. 111–184.

Møller, J., Toftaker, H., 2014. Geometric anisotropic spatial point pattern analysis and Cox processes. Scandinavian Journal of Statistics 41, 414–435.

Ohser, J., Stoyan, D., 1981. On the second-order and orientation analysis of planar stationary point processes. Biometrical Journal 23, 523–533.

Platt, W. J., Evans, G. W., Rathbun, S. L., 1988. The population dynamics of a long-lived conifer (Pinus palustris). The American Naturalist 131, 491–525.

Ripley, B. D., 1977. Modelling spatial patterns (with discussion). Journal of the Royal Statistical Society, Series B 39, 172–212.

Ripley, B. D., 1988. Statistical Inference for Spatial Processes. Cambridge University Press, Cambridge.

Stoyan, D., Kendall, W. S., Mecke, J., 1995. Stochastic Geometry and its Applications, 2nd Edition. Wiley, Chichester.

Stoyan, D., Stoyan, H., 1994. Fractals, Random Shapes and Point Fields: Methods of Geometrical Statistics. Wiley, Chichester.

Stoyan, D., Stoyan, H., 1996. Estimating pair correlation functions of planar cluster processes. Biometrical Journal 38, 259–271.

Tscheschel, A., Chiu, S. N., 2008. Quasi-plus sampling edge correction for spatial point patterns. Computational Statistics and Data Analysis 52, 5287–5295.

Tscheschel, A., Stoyan, D., 2006. Statistical reconstruction of random point patterns. Computational Statistics and Data Analysis 51, 859–871.

Zhang, T., Zhou, B., 2014. Test for the first-order stationarity for spatial point processes in arbitrary regions. Journal of Agricultural, Biological, and Environmental Statistics 19, 387–404.